Journal of Thermal Analysis and Calorimetry, Vol. 85 (2006) 2, 409–415

CRYSTALLIZATION AND MELTING BEHAVIOUR OF POLY(*m*-XYLENE ADIPAMIDE)

*B. B. Doudou**, *E. Dargent and J. Grenet*

Laboratoire PBM, UMR 6522, Equipe LECAP, Université de Rouen, Institut des Matériaux, Avenue de l'Université
B.P. 12, 76801 Saint Etienne du Rouvray Cedex, France

The melting and crystallisation behaviour of poly(*m*-xylene adipamide) (MXD6) are investigated by using the conventional DSC, X-ray diffraction and polarised light microscopy. Triple, double or single melting endotherms are obtained in subsequent heating scan for the samples after isothermal crystallisation from the melt state at different temperatures. The lowest melting peak can be ascribed to the melting of secondary crystals. The melting of primary crystals causes the medium melting peak and the highest melting peak is attributed to the melting of recrystallised species formed during heating. Following the Hoffman–Weeks theory, the equilibrium melting temperature is equal to 250°C and the equilibrium melting enthalpy ΔH_m^0 to 175 J g^{-1}. Then, using the Lauritzen–Hoffmann theory of secondary crystallisation, the analyse of the spherulitic growth shows that the temperature of transition between the growing regimes II and III is equal to 176°C. Finally the Gibbs-Thomson relationship allows the determination of the distribution function of crystalline lamellae.

Keywords: *crystallisation behaviour, melting behaviour, poly(m-xylene adipamide)*

Introduction

Poly(*m*-xylene adipamide) (MXD6) is one of the crystalline polyamide resins. It is produced through polycondensation of *meta*-xylene diamine with adipic acid. It has many distinguished properties compared with other conventional polyamide resins such as nylon 6 and nylon 66 [1]. One of the most remarkable properties of MXD6 concerns its superior gas barrier properties against dioxygen and carbon dioxide which are better than those of ethylene-vinylalcohol copolymers (EVOH), acrylonitrile copolymers (PAN) and vinylidenechloride copolymers (PVDC) under practical condition. For these reasons, the MXD6 has been widely applied for packaging materials, molding compounds and monofilaments [2]. For instance, it is used by blending or by multilayer techniques [3] to improve the gas-barrier properties of poly(ethylene terephthalate) (PET) in bottling industries.

Studies of the crystallization and of the melting behaviour of MXD6 have not been accomplished until recently. For this reason, we have these behaviours under isothermal conditions. Although industrial processes such as extrusion, injection molding and film production usually proceed under dynamic non-isothermal crystallization conditions, other studies have shown that data obtained from isothermal experiments are in agreement with those obtained under non-isothermal conditions [4–6]. Moreover, measurements of crystal growth rates are generally conducted in isothermal conditions [7].

In this paper, we have investigated the melting behaviour of isothermally crystallized MXD6 and a usual thermodynamic analysis was used to obtain the energetic parameters. The crystallisation processes, the morphology and the crystal growth of MXD6 are also studied by thermal analysis.

Experimental

Materials

MXD6 (6007) used in this study is supplied by Mitsubishi Gas Chemical Co; the number-average-molecular mass is 25000 g mol^{-1}; the density is 1.22 g cm^{-3}. The unit cell of the crystalline phase is triclinic and the parameters are: a=1.201 nm, b=0.483 nm, c=2.98 nm, α=75°, β=26°, γ=65° [8]. This is the only aliphatic polyamide resin containing *meta*-xylene groups (Fig. 1).

Methods

Wide angle X-ray diffraction measurements

XRD measurements are carried out by reflection at room temperature with a Kigaru miniflex diffractometer

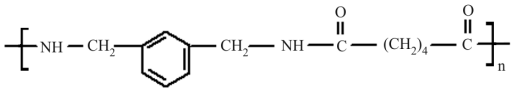

Fig. 1 Repeating unit of MXD6

* Author for correspondence: bessem.bendoudou@etu.univ-rouen.fr

1388–6150/$20.00

Akadémiai Kiadó, Budapest, Hungary
Springer, Dordrecht, The Netherlands

system using a Cu anode as X-ray source (λ=0.154 nm). Data are collected in the range of 10–50° (2θ) using 0.02° step and a counting time of 5 s.

Thermal analysis

The melting behaviour of MXD6 samples is investigated by conventional DSC (Perkin–Elmer DSC7). The melting temperatures are measured at the extremum of the corresponding peaks. This unusual procedure is principally forced by the overlap of three melting phenomena which impedes the determination of the onset as well as of the end of peaks; it is impossible to determine the first or the last trace of fusion. Then this procedure is the least bad method to measure a melting point.

Prior any in situ isothermal crystallisation, the samples are heated up to 300°C at 10°C min^{-1} and maintained at this temperature during 5 min to erase previous thermal histories. Then, they were rapidly cooled down to the selected temperatures where they were isothermally crystallised during various periods. After this crystallisation stage, the samples are rapidly cooled down to room temperature and finally, they are heated and analysed at 10°C min^{-1}.

The sample mass is equal to 10±1 mg and all the DSC runs are carried out under nitrogen atmosphere to minimise oxidative degradation. Before any experiment, the baseline is recorded using empty aluminium pans (reference and sample), and the calorimeter is calibrated by using melting temperature and enthalpy of a high purity indium standard (156.6°C and 28.45 J g^{-1}).

Crystallisation kinetics

Isothermal spherulitic growth rates of MXD6 are measured using a polarised light microscopy (Leica DM LM) equipped with a LinKam hot stage (CI94) and a video recording system. Samples are prepared by melting and crystallising the MXD6 sample into aluminium pans using a similar thermal protocol: 1) heating ramp up to 300°C, 2) isothermal holding during 5 min to erase thermal history, 3) fastest cooling down to the crystallisation temperature between 150 and 200°C and crystallisation (because the air cooling of the LinKam stage, the cooling rate was estimated to 20°C min^{-1}; this is the difference between both protocols) and 4) isothermal crystallisation. During the stage 4, the spherulites radii are measured directly from the video-recorded image. Finally the spherulitic growth rates are determined from the slopes of radii *vs.* time plots.

Results and discussion

Melting behaviour of MXD6

Before any DSC analyse of crystallised MXD6 samples, Fig. 2 presents the DSC trace of a heating run carried out on a fully amorphous sample (it was judged amorphous regards with the lack of X-ray diffraction peaks). Evidenced by the endothermic heat capacity jump ΔC_p, the glass transition appears for 78°C<T_g<93°C, the thermal cold crystallisation is revealed by an exothermic phenomenon lying between 125 and 160°C, then a second exothermic phenomenon appears around T=205°C. Finally, the melting of the crystalline phase is revealed by an endothermic peak occurring between 210 and 244°C. For polymers showing similar DSC data variations, the exothermic peak located just below the endotherm is generally attributed to a polymorphism [9] or to a crystalline reorganisation [10]. In order to investigate the crystalline structure of MXD6 isothermally crystallised from the melt at different temperatures, XRD measurements were carried out. Figure 3 shows the XRD patterns for three various crystallisation temperatures. Obviously, each sample exhibits six peaks at 2θ=14, 18.9, 21, 21.6, 23 and 25.6°, corresponding to the reflection of planes (002), (100), (010), (0$\bar{1}$2), (011) and (11$\bar{1}$) respectively. The third thermal crystallisation tempera-

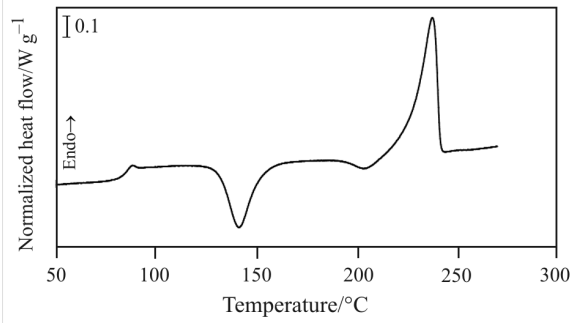

Fig. 2 DSC curve of a fully amorphous MXD6 sample (the heat flow is normalized to 1 g of matter)

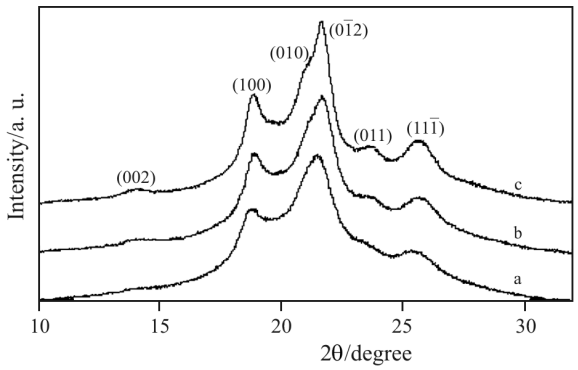

Fig. 3 XRD curves of MXD6 annealed at: a – 120°C, b – 200°C and c – 209°C

ture (T_c=209°C) was chosen just above the second exothermic peak in such a way that if any change in the crystalline parameters occurs during this exotherm, one can expect modifications of the corresponding XRD pattern. It is clear in Fig. 3 that the crystallisation temperature did not affect the position of these peaks and the crystalline parameters. As a consequence, the secondary exotherm peak is quite probably due to a crystalline reorganisation. Indeed, when the sample is crystallised at low temperature, the crystals are ill-formed and then relatively prone to be re-organised during heating to a crystal population having a higher thermodynamic stability.

Figure 4 shows DSC thermal phenomena for MXD6 samples recorded after complete crystallisation from the melt state at various crystallisation temperatures ranging from 150 to 200°C. Either double or triple-melting endotherm and one exotherm peak are observed. These endothermic peaks are labelled I, II and III for lowest, medium and highest temperature melting endotherms, respectively and the temperatures at maxima will be therefore denoted T_I, T_{II} and T_{III} in an increasing order.

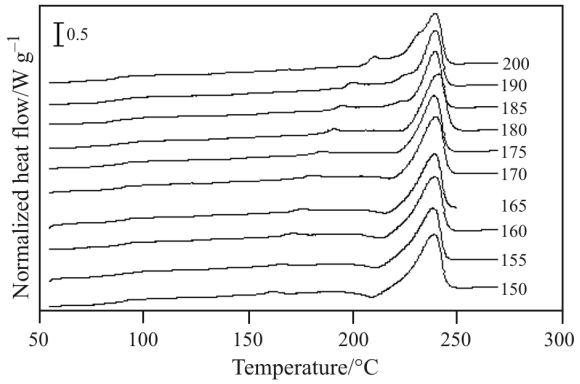

Fig. 4 Melting endotherms (normalized to 1 g) of MXD6 recorded with a heating rate of 10°C min^{-1}, after complete isothermal crystallisation at the specified temperatures

These results show clearly that the melting behaviour strongly depends on the crystallisation temperature T_c. For the lower side of the studied domain (T_c<185°C) two endothermic melting peaks and a single exothermic peak are evidenced whereas for the upper side, the exothermic peak disappears and the three melting endothermic peaks are only present. Figure 5 reports the variations of melting temperatures as a function of crystallisation temperature and clearly shows that both peaks I and II move towards higher temperatures as the crystallisation temperature increases while peak III seems to be independent on the crystallisation temperature. Added to the presence of the exotherm, this stability suggest to allocate the endotherm III to the melting of the recrystallised crys-

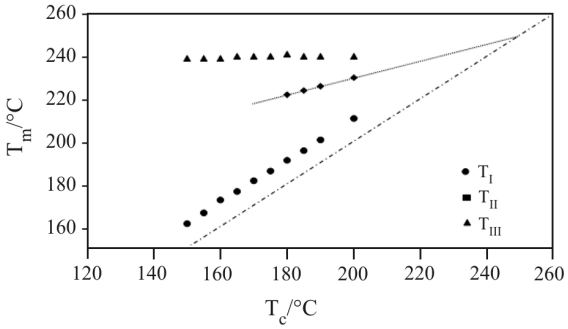

Fig. 5 Variation with the crystallisation temperature T_c of lowest, intermediate and highest melting temperatures (T_I, T_{II}, T_{III}) as determined after complete crystallisation from the melt state. The dashed line (- - -) shows T=T_c and allows the location of the melting temperature. The dotted line (· · ·), linear regression of T_{II} *vs.* T_c

tallites [11, 12]. At this place of the text, let us notice that the difference between T_I and T_c is appreciably constant and equal to 12±0.5°C whatever the temperature of crystallisation. The DSC scans reported Fig. 6 show the gradual evolution of the crystalline reorganisation with the duration of the isothermal crystallisation carried out at T_c=201°C. T_I shifts to higher temperature with increasing crystallisation times and the magnitude of peak II increases with time and whereas this of peak III decreases. As shown in Fig. 7, T_I increases linearly with the logarithm of the crystallisation duration. This kind of dependence is conventionally associated with secondary crystallisation [13, 14]. Then we can attribute the endotherm I to the melting of secondary lamellae.

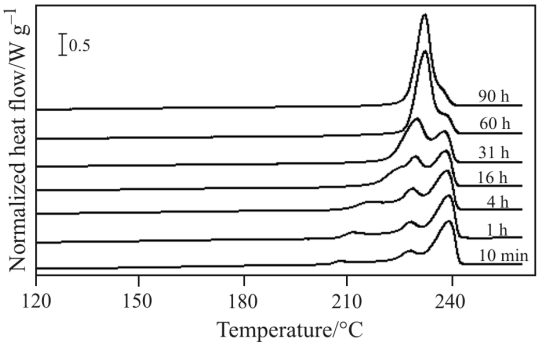

Fig. 6 Melting endotherms (10 K min^{-1}) of MXD6 samples after crystallisation at 201°C for different durations (as indicated)

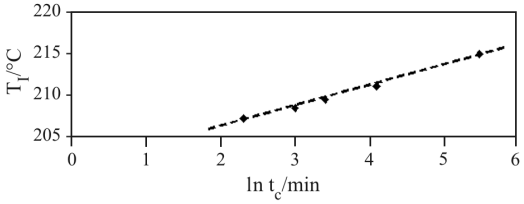

Fig. 7 The dependence of T_I on crystallisation duration

The middle melting endotherm II clearly increases with crystallisation time (Fig. 6) whereas the magnitude of the endotherm III which is due to the melting of recrystallised crystallites decreases. Finally, endotherms II and III merge for the sample after 90 h of crystallisation. This reveals that a larger fraction of the MXD6 molecules can crystallise into more perfect crystals when the crystallisation time is increased, and that the fraction of material able to re-crystallise is reduced relatively. As it is known that at the highest crystallisation temperatures and for the longest durations primary crystals are favoured [15, 16], endotherms II are considered to be characteristic of the melting of the crystals formed during the primary crystallisation.

For a better understanding of the crystallisation behaviour, the MXD6 crystal growth rate was studied with the help of the Hoffman and Lauritzen theory. But first and foremost, it is necessary to determine the equilibrium thermodynamic parameters of the polyamide.

Equilibrium thermodynamic parameters

Up to now, the equilibrium melting enthalpy ΔH_m^0 and the equilibrium melting temperature T_m^0 of MXD6 have not been yet determined and are not available from literature. However, it is necessary to know ΔH_m^0 to calculate the degree of crystallinity of the material. In the same way, it is necessary to know T_m^0 to determine the size of the crystals and to understand the supercooling dependence of the multiple melting peaks of MXD6. These parameters will be classically determined by extrapolation.

Equilibrium melting enthalpy

On the one hand, there is a linear relationship between the total degree of crystallinity X_c of sample the enthalpic quantity (ΔH_m–ΔH_c) [15]:

$$X_c = \frac{1}{\Delta H_m^0}(\Delta H_m - \Delta H_c) \quad (1)$$

where ΔH_m and ΔH_c are the melting and cold crystallisation enthalpies obtained by DSC measurement respectively (Fig. 2). On the other hand, this degree could be obtained by resolving the overlapping of crystalline peaks of X-ray diffraction with Gaussian functions [17]. Figure 8 shows the plot of (ΔH_m–ΔH_c) *vs.* X_c for MXD6 samples and the linear least square fit. The slope of this straight line provides the evaluated value of ΔH_m^0: 175±10 J g^{-1}. This value is close to the values of ΔH_m^0 available in literature for other polyamides: PA 6-6 (188.3 J g^{-1}) [15], PA 6-10 (211.7 J g^{-1}) [18] and PA 10-10 (244.0 J g^{-1}) [19].

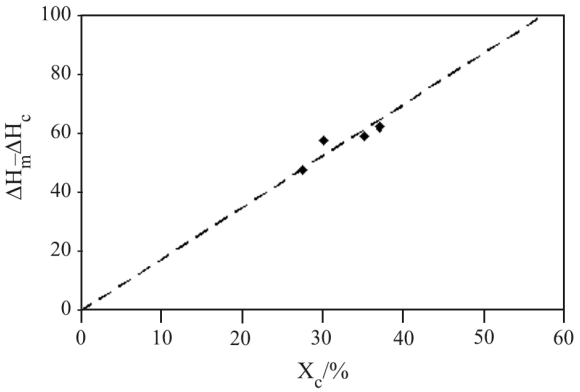

Fig. 8 (ΔH_m–ΔH_c) *vs.* X_c for MXD6 samples; X_c from X-ray diffraction, ΔH_m and ΔH_c from DSC measurements

Equilibrium melting temperature

According to a theory derived by Hoffman and Weeks [20] (also known as the linear Hoffman–Weeks extrapolation), the equilibrium melting temperature T_m^0, which is the melting temperature of infinitely thick crystallites, can be estimated at the intercept of the linear extrapolation of the variations of the melting temperature T_m *vs.* crystallisation temperature T_c and of the line T_m=T_c. Mathematically, this could be expressed by the equation:

$$T_m = \frac{T_c}{2\beta} + T_m^0\left[1 - \frac{1}{2\beta}\right] \quad (2)$$

where β (=L_c/L_c^*) is the 'thickening ratio'; in other words β indicates the ratio of the thickness of the mature crystallites L_c to that of the initial ones L_c^*. It is always supposed to be greater than or equal to 1. As shown in the experimental part, the peaks of type II correspond to the melting of primary crystals. Then the temperature at the maximum of these peaks could be considered equal to T_m in the determination of T_m^0. As already displayed in Fig. 6, T_{II} varies linearly with T_c, at least within the temperature range of interest. The intersection of the least-squared fit (T_{II} *vs.* T_c) with the line T_m=T_c provides the values of T_m^0. Then, T_m^0 is evaluated to be equal to 250±2°C which is relatively close to the values of PA 6-6 (280°C) [15], PA 6-10 (238°C) [18] and PA 10-10 (214°C) [19] noticed in literature.

Isothermal crystallisation behaviour of MXD6

Figure 9 shows spherulite-shaped crystallites of MXD6 isothermally crystallised at 180°C observed by polarised light microscopy. At constant temperature, the plot of the spherulite radii *vs.* time of crystallisation allows the determination of the spherulitic growth rate G (Fig. 10). According to the shape of the curves, one can suppose that the radius of spherulite increases linearly with time until the

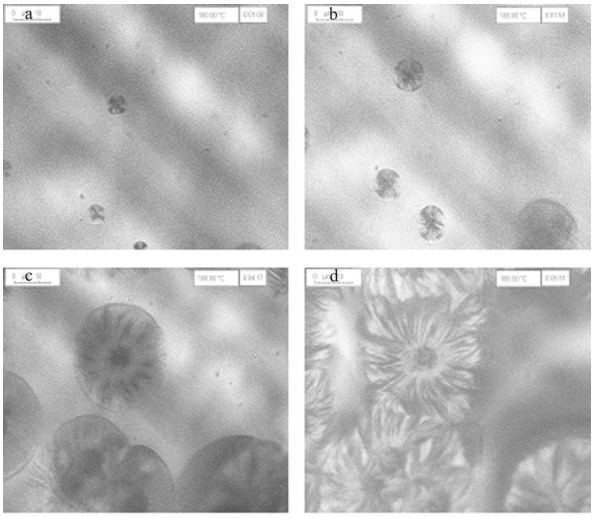

Fig. 9 Polarised light micrographs of MXD6 isothermally crystallised at 180°C; crystallisation durations: a – 68 s; b – 113 s; c – 257 s; d – 351

spherulites touch on each other and G is given by the slope of the mean square straight line fit. As shown in Fig. 11, the spherulitic growth rate increases when the crystallisation temperature decreases. As already mentioned in the experimental part §2.4, it should be noticed that due to weakness of the possible highest cooling rate (≈20 K min^{-1}), it is impossible to get a fully amorphous sample at low temperature. Therefore it is difficult to explore the whole temperature domain. This could be observed in Fig. 10 where for the lowest crystallisation temperatures the lines radii *vs.* time do not go through the origin showing the existence of initial crystallites. However, these initial crystallinity do not modify the spherolitic growth rate at least as long as crystallites do not overlap.

Lauritzen and Hoffman [21] in their secondary nucleation kinetics theory of polymer crystal growth suggest that the polymer crystallise in three different regimes and that a crystallisation regime depends on two processes: the first one consists into the deposition of the secondary nucleus on the growing face and the second one corresponds to the lateral spreading of polymer chains or segments of chain across the face. The regime I occurs when the lateral spreading rate is greater than that of the surface nucleation rate. The regime II is observed when the rates of the two processes are comparable while the regime III occurs when the rate of secondary nucleation is greater than these of the lateral spreading. Fundamentally, a transition between regimes is observed as a break in the growth rate data according to the crystallisation temperature or, to be exact, the degree of supercooling. In other words, the regime I is observed at the highest temperatures. At moderate supercoolings, the regime II is observed. Finally the regime III is observed [22] when the supercooling is further continued. Due to the relationship of the growth rate with the secondary nucleation rate in all the regimes, it is obvious that one should observe a downward break in the growth rate data at the point where the regimes I–II transition occurs, and an upward break for the regimes II–III transition. In this context, the linear growth rate G of the spherulitic growth of MXD6 is given by the following equation:

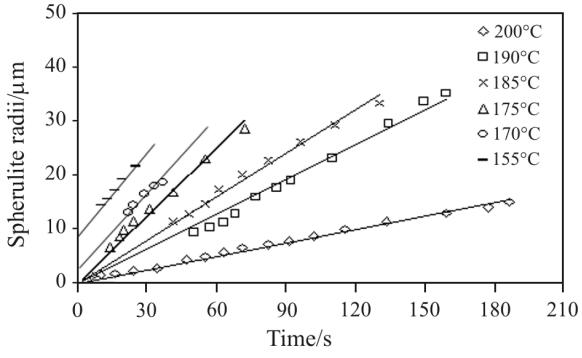

Fig. 10 Plots of radius of spherulite *vs.* crystallisation time when the sample is isothermally crystallised at different temperatures

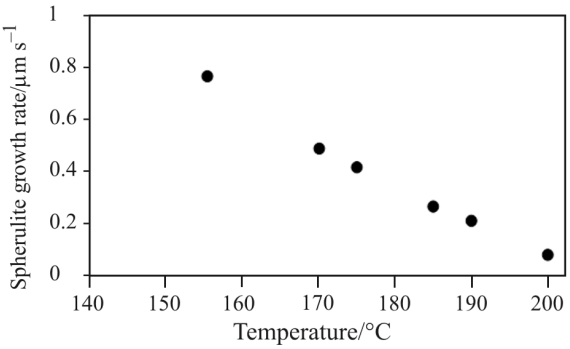

Fig. 11 Plot of spherulitic growth rate of MXD6 *vs.* crystallisation temperature. The spherulitic growth rate is determined from the slope of the plots of radii *vs.* time in Fig. 9

$$G = G_0 \exp\left(\frac{-U^*}{R(T_c - T_\infty)}\right)\exp\left(\frac{-K_g}{fT_c\Delta T}\right) \qquad (3)$$

where G_0 is a pre-exponential factor which is not strongly dependent on temperature, U^* is the activation energy for the transportation of segments of molecules across the melt/solid surface interface and is usually equal to 6279 J mol^{-1} (1500 cal mol^{-1}), R is the gas constant, T_∞ is the temperature below which all viscous flow $\{T_\infty = T_g - 30\}$, ΔT is the degree of supercooling defined by $T_m^0 - T_c$, f $\{=2T_c/((T_m^0 + T_c)\}$ is a correction factor which accounts for the variation in the heat of fusion of perfect crystal with temperature, and K_g is the nucleation exponent defined as

$$K_g = \frac{\xi b_0 \sigma \sigma_e T_m^0}{k_B \Delta H_f^0} \quad (4)$$

where ξ=2 for regime II (intermediate temperatures) and 4 for regimes I (high temperature) or III (low temperature), b_0 denotes the crystal layer thickness along the growth direction, σ and σ_e are the lateral and fold surface free energies respectively. T_m^0 is the equilibrium melting temperature, k_B is the Boltzmann's constant, and ΔH_f^0 the equilibrium melting enthalpy per unit volume for a fully crystalline polymer $\{\Delta H_f^0 = \Delta H_m^0 \rho_c\}$. It is often convenient to rearrange Eq. (3) as the following equation:

$$\ln G + \frac{U^*}{R(T_c - T_\infty)} = \ln G_0 - \frac{K_g}{f T_c \Delta T} \quad (5)$$

when the value of the left-hand side of (5) is plotted *vs.* $1/(fT_c\Delta T)$ the nucleation exponent (K_g) is equal to the slope of the plot. Figure 12 shows a transition between regime II and III in the vicinity of 176°C. Then, the slopes of the fits lead to $K_g(II)=2.1\cdot10^5$ and $K_g(III)=4.4\cdot10^5$. The ratio of $K_g(III)$ to $K_g(II)$ equal to 2.1, is close to 2.0 as predicted by the Lauritzen–Hoffman theory.

Prior to the determination of crystal thickness, it is necessary to calculate free energies σ_e and σ of the fold and the lateral surfaces respectively. Using Eq. (5), σ_e could be determined from K_g value. With b_0=0.483 nm, T_m^0=250°C, a crystal density ρ_c=1.21 g cm^{-3} and ΔH_f^0=211.75 J cm^{-3}, $\sigma\sigma_e$ is estimated to be equal to $1203\cdot10^{-14}$ J^2 cm^{-4}. The lateral surface-free energy σ may be estimated by the empirical relation of Thomas–Stavely [23]:

$$\sigma = \alpha \Delta H_f^0 (a_0 b_0)^{1/2} \quad (6)$$

where a_0 is the molecular width, and α is an empirical constant usually assumed to be equal to 0.1. Thus σ can be estimated to be $16.1\cdot10^{-7}$ J cm^{-2} and finally the fold surface free energy σ_e to $74.6\cdot10^{-7}$ J cm^{-2}.

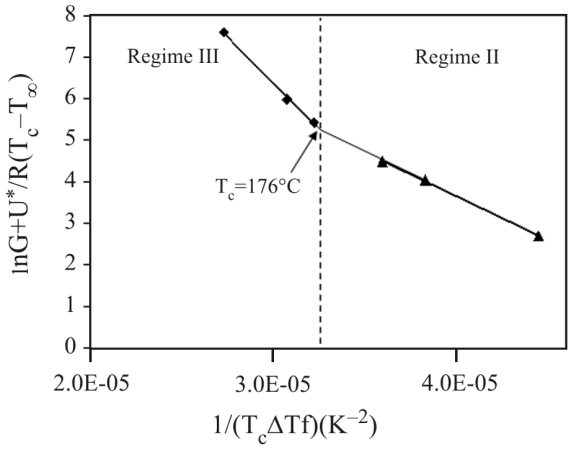

Fig. 12 Analysis of the spherulitic growth rate of MXD6 using Lauritzen-Hoffman theory of secondary crystallisation

Determination of crystalline lamellae thickness

The thickness e is based on the approximate expression of Gibbs-Thompson giving the depletion of the melting point with the thickness [15]:

$$T_m = T_m^0 \left(1 - \frac{2\sigma_e}{e \Delta H_m^0 \rho_c}\right) \quad (7)$$

where T_m and T_m^0 are the melting temperatures of a lamella of thickness e and the equilibrium melting temperature respectively. The relation of Gibbs-Thompson, which supposed that the lamella thickness e of crystals is very small compared to other dimensions and the melting of crystals occurs without reorganization at the equilibrium, is particularly appropriate for polymers crystallised in a spherulitic form. From DSC melting curve and thanks to this relationship, Fig. 13

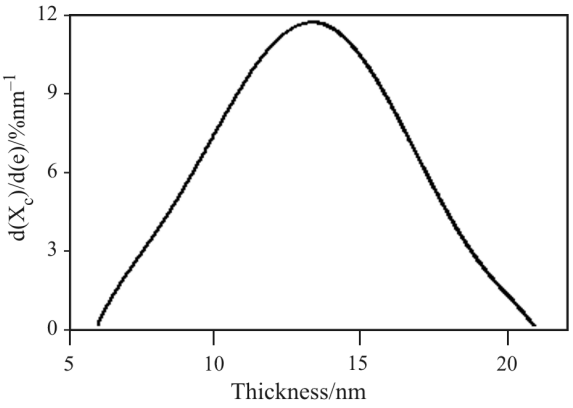

Fig. 13 Distribution function d(X_c)/d(e) of crystalline lamellae thickness

shows the distribution function thickness of lamellae centred on 13–15 nm; this distribution is similar to these already observed for PET which has the same unit cell and the same melting behaviour [24, 25].

Conclusions

This work deals with the crystallisation and melting behaviours of the polyamide MXD6 under isothermal conditions. Samples after isothermal crystallisation from the molten state at different temperatures, triple, double or single melting endotherms were obtained in subsequent heating scan of the samples. The endotherm I which appeared about 12°C above the crystallization temperature, was attributed to the melting of the crystals formed during the secondary crystalliza-

tion, intermediate endotherm II to the melting of the crystals formed during the primary crystallization and the highest endotherm III to those formed as a result of remelting of recrystallised crystallites. The spherulitic growth kinetics were analysed using the Lauritzen-Hoffman theory of secondary crystallisation. The equilibrium melting enthalpy and the equilibrium melting temperature were determined, respectively. With the help of the Gibbs-Thompson relationship, the distribution function of crystalline lamellae size could be determined.

References

1 Mitsubishi Gas Chemical Catalog, Nylon-MXD6: Superior performance in barrier packaging, p. 2.
2 Mitsubishi Gas Chemical Catalog, MX-Nylon (2000) p. 5.
3 Y. S. Hu, V. Prattipati, S. Mehta, D. A. Schiraldi, A. Hiltner and E. Baer, Polymer, 46 (2005) 2685.
4 M. L. Di Lorenzo, Polymer, 42 (2001) 9441.
5 M. Ren, Z. Mo, Q. Chen, J. Song, S. Wang, H. Zhang and Q. Zhao, Polymer, 45 (2004) 3511.
6 A. Dobreva, M. Alonzo, M. Gonzalez, A. Gonzalez and J. A. de Saja, Thermochim. Acta, 258 (1995) 197.
7 B.Wunderlich, Macromolecular Physics, Crystal Nucleation, Growth, Annealing, Vol. 2. New York: Academic Press, 1976.
8 A. Miyamoto, Nylon-MXD6, in Polymer Data Handbook, Oxford University Press 1999, p. 230.
9 H. Yoshida, Thermochim. Acta, 267 (1995) 239.
10 O. Persyn, V. Miri, J. M. Lefebvre, C. Depecker, C. Gors and A. Stroeks, Polym. Eng. Sci., 44 (2004) 261.
11 M. Y. Ju and F. C. Chang, Polymer, 42 (2001) 5037.
12 Y. Wang, M. Bhattacharya and J. F. Mano, accepted in J. Polym. Sci. Part B: Polym Phys.
13 Y. Kong and J. N. Hay, Polymer, 44 (2003) 623.
14 G. C. Alfonso, E. Pedemonte and L. Ponzetti, Polymer, 20 (1979) 104.
15 B. Wunderlich, Macromolecular Physics, Crystal Melting, Vol. 3, New York: Academic Press 1980.
16 Z. G. Wang, B. S. Hsiao, B. B. Sauer and W. G. Kampert, Polymer, 69 (1999) 4615.
17 M. Kattan, E. Dargent, J. Ledru and J. Grenet, J. Appl. Polym. Sci., 81 (2001) 3405.
18 G. M. Wang, D. Y. Yan and H. S. Bu, Chin. Polym. Bull., 4 (1991) 199.
19 Z. S. Mo, Q. B. Meng and J. H. Feng, Polym. Int., 32 (1993) 53.
20 J. D. Hoffman and J. J. Weeks, J. Res. Natl. Bur. Stand., A66 (1962) 13.
21 J. D. Hoffman, G. T. Davis and J. I. Lauritzen, In: Hannay HB editor, Treatise on Solid State Chemistry, Vol. 3, New York, Plenum, 1975. Chapter 7.
22 P. Supaphol and J. E. Spruiell, Polymer, 41 (2000) 1205.
23 D. G. Thomas and L. A. K. Stavely, J. Chem. Soc., (1952) 4569.
24 X. F. Lu and J. N. Hay, Polymer, 42 (2001) 9423.
25 E. Dargent, University of Rouen, P.h.D. 1994.

Received: August 22, 2005
Accepted: May 26, 2006

DOI: 10.1007/s10973-005-7299-y